Dynamics in resonant x-ray emission of the core exciton state: Competition between electron itinerancy and lattice relaxation

Satoshi Tanaka[1,*] and Yosuke Kayanuma[2]
[1]*Department of Materials Science, Osaka Prefecture University, Sakai, 599-8531, Japan*
[2]*Graduate School of Engineering, Osaka Prefecture University, Sakai, 599-8531, Japan*
(Received 27 August 2004; published 31 January 2005)

Resonant x-ray emission spectrum from the core exciton state is theoretically investigated for a model of one-dimensional covalent crystals. A theoretical prescription for the calculation of core level sepctra is proposed in the model, where both the effects of the electronic itinerancy and the electron-phonon coupling in the core excited state have been quantum mechanically treated. The dynamical changeover from a weak- to a strong-coupling regime as the phonon relaxation proceeds is well reflected in the resonant x-ray emission spectrum.

DOI: 10.1103/PhysRevB.71.024302 PACS number(s): 78.70.En, 71.38.−k, 78.20.Bh

I. INTRODUCTION

Resonant x-ray emission spectroscopy is a powerful tool for revealing the relaxation dynamics in the core-excited states. Since the lifetime of the core hole is very short (~fs) due to the ultrafast Auger decay, it has long been presumed that only the electronic processes take part in the relaxation dynamics in the core-excited state. The finding of the existence of large lattice relaxation in the core exciton state in some materials is, therefore, a remarkable progress in recent years.[1–3]

A decade ago, Ma and his coworkers showed in their pioneering work that the resonant x-ray recombination emission spectrum in diamond has a long, low energy tail,[1] which indicates that a strong lattice deformation is taking place in the core-excited state. Quite recently, Harada *et al.* succeeded in precisely measuring the resonant x-ray emission spectra in graphite including their polarization dependence.[2] The experimental data have decisively shown that a large atomic displacement is induced in the σ^*-core exciton state of graphite. In addition, the observed strong polarization dependence of the x-ray emission line shape indicates that the local symmetry around the core-excited atom is broken by the vibronic coupling with the asymmetric phonon mode. The evidence of strong lattice relaxation has also been reported for N 1*s* recombination emission spectrum of $LiNO_3$ crystals.[3] Also in free molecules, e.g., BF_3, CF_4, etc., the energy splittings of the core excited states due to the vibronic Jahn-Teller couplings have been observed in the x-ray absoprtion, resonant Auger emission, and resonant x-ray emission spectra.[4–9] It may well be conjectured that such a large atomic displacement effect is a universal characteristic for light element materials in which the 1*s* core hole has a relatively long lifetime (~10 fsec) and the phonon frequency is relatively high.

The present authors theoretically analyzed the experimental data by the vibronic cluster model,[2,10] in which the quantum effect of the coupled phonon mode is fully taken into account. It proved that the essential features of the x-ray emission line shape are well reproduced by the small cluster model strongly coupled with localized phonon modes. The localized nature of the core-exciton state allows us to treat the dynamical processes by a molecular-like picture in the first order approximation; however, there still remains a problem if one examines the whole optical processes of the x-ray absorption and the x-ray emission. In the experimental data of the x-ray absorption spectra of diamond[1,11,12] and graphite,[13–16] the core exciton has a relatively sharp peak structure below the conduction band edge. This indicates that the effective electron-phonon coupling is weak in the final state of the x-ray absorption, in contradiction with the strong coupling model. This apparent discrepancy can be resolved by taking into account the dynamical aspect of the lattice relaxation correlated with the electron itinerancy. Just after the x-ray absorption, the wave function of the core exciton is relatively diffused, so that the effective electron-phonon coupling is weak. But as the lattice deformation goes on, the wave function shrinks, and the effective coupling constant increases cooperatively. The changeover from shallow to deep level of the core exciton state has been treated in our previous paper by a simplified model.[17]

In the present work, we extend our study on the dynamical aspect of lattice relaxation of core excitons. In contrast to the previous work, the more or less realistic nature of the core exciton state in semiconductors is taken into account here. It is important to notice that the Γ-point of the conduction band of diamond or σ^*-band of graphite has a *s*-like symmetry composed of antibonding states of *sp* hybridized orbitals. Therefore, the optical transition from the 1*s* core state to the *s*-like bound state is dipole forbidden, and the coupling with the asymmetric local phonon mode becomes important. As a first step, we show in the present work a formulation and the numerical results of the line shape analysis of the x-ray absorption and the resonant x-ray emission spectra for a one-dimensional model of core excitons in semiconductors. It is shown that as long as the localized core exciton is coupled with the local phonon mode, the effect of the electron itinerancy is easily incorporated into the vibronic model, in which the quasi Jahn-Teller effect is quantum mechanically treated. It follows that the wave function of the core exciton state eventually shrinks after the relaxation, which is well reflected in the resonant x-ray emission spectrum.

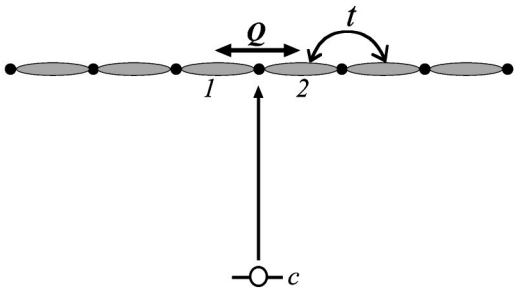

FIG. 1. One dimensional chain of the antibonding conduction states. A core electron c is excited to the antibonding orbitals 1 and 2 around the excited atom.

II. MODEL

We consider a resonant x-ray emission process of the covalent semiconductors, like graphite and diamond. For simplicity we consider a one-dimensional, covalent crystal. In the process the 1s core electron is excited to the conduction band characterized by the sp hybridized, antibonding, unoccupied state. The x-ray emission takes place through the recombination radiative deexcitation of the excited electron to the 1s core level. The model Hamiltonian for the initial and final states of the transition is given by ($\hbar=1$ hereafter)

$$\hat{H}_g = \epsilon_c a_c^\dagger a_c + (1/2)(\hat{P}^2 + \omega^2 \hat{Q}^2), \tag{1}$$

where a_c is the annihilation operator for the 1s core electron with energy ϵ_c. The coordinate and the momentum operators of the local phonon mode with frequency ω, which is coupled with the core exciton state, are denoted by $\hat{Q}$ and $\hat{P}$, respectively. The spin degrees of freedom are neglected.

In the intermediate state, the core electron is excited to the antibonding states, labeled by 1 and 2, around the excited atom (Fig. 1). The excited electron itinerates between the antibonding orbitals by the transfer t, and the core hole exerts the attractive Coulomb potential v on the excited electron, which is assumed to be a local interaction. In addition, the excited electron is coupled with the local antisymmetric vibration $\hat{Q}$. Therefore the Hamiltonian for the intermediate state reads

$$\hat{H}_e = \hat{H}_0 + \hat{V} \tag{2a}$$

$$\hat{H}_0 = -t\sum_{\langle i,j\rangle} a_i^\dagger a_j + \frac{1}{2}(\hat{P}^2 + \omega^2 \hat{Q}^2) \tag{2b}$$

$$= \sum_k \epsilon_k a_k^\dagger a_k + \frac{1}{2}(\hat{P}^2 + \omega^2 \hat{Q}^2) \tag{2c}$$

$$\hat{V} = -v(a_1^\dagger a_1 + a_2^\dagger a_2) - \sqrt{2\omega}\alpha \hat{Q}(a_1^\dagger a_1 - a_2^\dagger a_2), \tag{2d}$$

where a_i denotes the annihilation operator of the antibonding state i, and α is the coupling constant of the antibonding states 1 and 2 with the local phonon mode $\hat{Q}$. In Appendix A we show how the tight binding Hamiltonian of a one-dimensional semiconductor can be reduced to the one-band model described by Eq. (2b). In Eq. (2c), a_k is the electron annihilator in the k-representation and ϵ_k represents the energy dispersion

$$\epsilon_k = -2t\cos kd, \tag{3}$$

where d is the lattice constant. The effect of the energy dissipation of the local phonon mode is neglected here. This is justified for the case of the core excited state because the lifetime of the excited state is very short.

Note that the suffix i in the Hamiltonian (2b) represents not the *site* of the atom but the antibonding *orbital* between two atoms, which is composed of the sp-hybridized atomic orbitals. The conduction band is formed by the intra-atomic electron transfer. This is a simplified one-band, tight-binding model of the conduction band of covalent crystals. The vibronic interaction in Eq. (2d) then represents the modulation of the energies of the antibonding orbitals around the core-excited atom due to the antisymmetric translational mode.

The 1s core electron makes a transition by the x-ray irradiation to the unoccupied p-orbital. Since the p-component of the hybridized orbital is proportional to the difference of the states $|1\rangle$ and $|2\rangle$, the transition operator is given by

$$\hat{M} = (a_1^\dagger - a_2^\dagger)a_c + \text{h.c.}, \tag{4}$$

aside from irrelevant factors.

We calculate the probability $I(\Omega_1,\Omega_2)$ that a photon with energy Ω_1 is absorbed and a photon with energy Ω_2 is emitted at a low temperature well below $\hbar\omega/k_B$. The probability is given by

$$I(\Omega_1,\Omega_2) = \sum_f \left| \sum_m \frac{\langle f|\hat{M}|m\rangle\langle m|\hat{M}|i\rangle}{E_i + \Omega_1 - E_m - i\gamma} \right|^2 \times \delta(E_i + \Omega_1 - E_f - \Omega_2), \tag{5}$$

where $|i\rangle$ is the ground state of H_g with energy E_i, $|f\rangle$ is an eigenstate of H_g with energy E_f, $|m\rangle$ is an eigenstate of H_e with energy E_m, and γ is the decay constant of the core hole. Any state of the electron-phonon system can be expanded in terms of the direct product basis set: $|\xi;n\rangle \equiv |\xi\rangle \otimes |n\rangle$, where $|\xi\rangle \equiv a_\xi^\dagger|v\rangle$, in which $|v\rangle$ is the vacuum of the electron and ξ runs over c (core state) and k (conduction band). $|n\rangle$ is the phonon number state ($n=0,1,2,\cdots$). The initial state is written as $|i\rangle=|c;0\rangle$ with energy ϵ_c, and the final states are $|c;n\rangle$ ($n=0,1,2,\cdots$), with energy $\epsilon_c+n\omega$. Here and hereafter, we neglect the zero point energy.

Substituting Eq. (4) into Eq. (5), we then have

$$I(\Omega_1,\Omega_2) = \sum_n \left| \sum_{i,j=1}^{2} G_n^{i,j}(\Omega_1 + \epsilon_c - i\gamma) \right|^2 \delta(\Omega_1 - \Omega_2 - n\omega), \tag{6}$$

where $G_n^{i,j}(z)$ with $z \equiv \Omega_1 + \epsilon_c - i\gamma$ is a phonon Green's function for the electronic states $|i\rangle$ and $|j\rangle$ defined by

$$G_n^{i,j}(z) \equiv \langle i,n|[1/(z-\hat{H}_e)]|j,0\rangle. \tag{7}$$

The Green's function $G_n^{i,j}(z)$ represents the electron transition from the j-th to i-th site with simultaneous n-phonon excitation.

Because of the symmetry, Eq. (6) is reduced to

$$I(\Omega_1,\Omega_2) = 4\sum_n |G_n^{1,1}(z) - G_n^{2,1}(z)|^2 \delta(\Omega_1 - \Omega_2 - n\omega). \quad (8)$$

Therefore, the x-ray emission spectrum reflects the probability of the scattering of the excited electron back to the excited atomic site accompanied with the simultaneous multiphonon excitations. As shown below, $G_n^{1,1}$ and $G_n^{2,1}$ are easily obtained because of the localized nature of the electron-phonon interaction.

Applying the Dyson equation to $\hat{H}_e$ in Eq. (2a),

$$\frac{1}{z-\hat{H}_e} = \frac{1}{z-\hat{H}_0} + \frac{1}{z-\hat{H}_0}\hat{V}\frac{1}{z-\hat{H}_e}, \quad (9)$$

we derive a recurrence formula for the phonon Green's function Eq. (7). The explicit expression of the equations are shown in the Appendix B. In the actual calculation, we truncate the successive hierarchy of the equations [Eq. (B5)] at a large phonon number state, confirming that the calculated results are not being influenced by the truncation. The simultaneous equations for $G_n^{i,j}(z)$ are then numerically solved by a conjugate gradient method.[18]

The x-ray absorption $I_a(\Omega)$ is obtained by using the solution of Eq. (B5), because the absorption is expressed in terms of Green's function:

$$I_a(\Omega) = \sum_m |\langle m|\hat{M}|i\rangle|^2 \frac{\gamma/\pi}{(E_i + \Omega - E_m + \gamma)^2} \quad (10a)$$

$$= \frac{1}{\pi}\mathrm{Im}\sum_{i,j=1}^{2} G_0^{i,j}(\epsilon_c + \Omega - i\gamma). \quad (10b)$$

Note that all of the information of the electronic band structure is included in the lattice Green's function

$$g(z) \equiv \frac{1}{z-\hat{H}_0}, \quad (11)$$

where $\hat{H}_0$ is given in Eq. (2b). For the one-dimensional, tight binding model treated here, the lattice Green's function is obtained as follows:

$$g_{i,i}(x) = [1/(B\sqrt{x^2-1})] \equiv g_0(z), \quad (12a)$$

$$g_{i,i+1}(x) = [(-x+\sqrt{x^2-1})/(B\sqrt{x^2-1})] \equiv g_1(z), \quad (12b)$$

where $x \equiv z/B$. These two lattice Green's functions are used in Eqs. (B3)–(B5).

III. NUMERICAL RESULTS

First we show the calculated results of the localized model in which the excited electronic states are essentially composed of $|1\rangle$ and $|2\rangle$ around the excited atomic site. The adiabatic potential curve along Q is shown in Fig. 2, where the origin of the energy is taken $-\epsilon_c$. The energy unit of the vertical axis is taken to be the unperturbed frequency of the local phonon mode ω, and the unit of length of the horizontal axis is $1/\sqrt{\omega}$. In the calculation, we used the parameters $\alpha=5$ and $B=0.1\omega$. The strong electron-phonon interaction gives a large relaxation energy $S=\alpha^2\omega=25\omega$. If we evaluate ω by a typical value of the light element materials, which is about 0.1 eV[2,6–8,10], this relaxation energy S amounts to ~2 eV, which is also in the range of the realistic values for these materials. Because of the finite B, the adiabatic potentials for the states $|1\rangle$ and $|2\rangle$ show an avoided crossing around $Q=0$, as shown in Fig. 2(b). At $Q=0$, we have two symmetrically different electronic eigenstates with respect to the inversion for the excited atomic site: the symmetric $|s\rangle=1/2(|1\rangle+|2\rangle)$ state and the antisymmetric $|p\rangle=1/2(|1\rangle-|2\rangle)$ state. To the lower and upper branches around $Q=0$ in Fig. 2(b) correspond the $|s\rangle$ and $|p\rangle$ states, respectively.

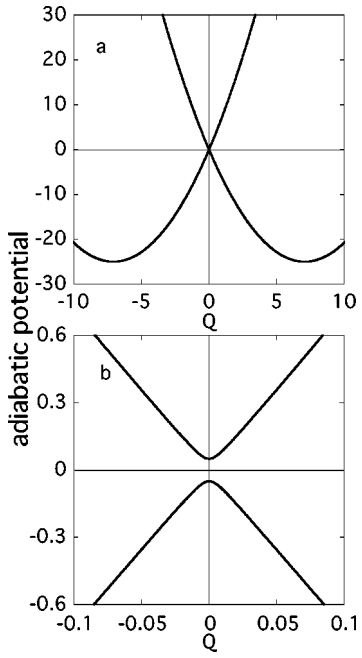

FIG. 2. Adiabatic potential curves along Q for the localized model: (a) overall feature and (b) expanded feature. The origin of the energy is taken $-\epsilon_c$. The energy unit of the vertical axis is taken to be the unperturbed frequency of the local phonon mode ω, and the unit of length of the horizontal axis is $1/\sqrt{\omega}$.

We show the calculated x-ray absorption spectrum for the localized model in Fig. 3(a). The spectrum shows a symmetric Gaussian line shape with a large width of about $2\alpha\omega=10\omega$, which is a typical spectral feature of the strong electron-phonon coupling system. The quasi-Jahn-Teller coupling which is due to the electronic transfer between the $|1\rangle$ and $|2\rangle$ states has an invisibly small effect on the absorption spectrum.

We show the calculated x-ray emission spectra of the localized model with the same parameter values in Figs. 3(b) to 3(d), where the horizontal axis is the Stokes shift from the excitation energies, which are marked by the arrows in Fig. 3(a). The emission spectrum (c) for the excitation to the absorption peak shows a typical line shape of the second order optical process of a localized center with a short lifetime.[19] It is composed of a strong Rayleigh line followed by a succession of higher order Raman lines. The gross structure of the line shape is, however, understood more naturally as a hot

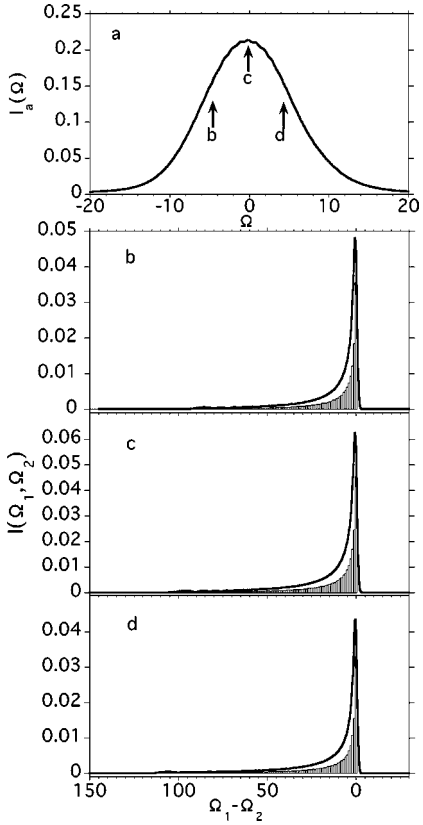

FIG. 3. Calculated results of x-ray absorption (a) and resonant x-ray emission spectra (b)~(d) of the localized model. In (a) the horizontal axis is x-ray energy for which the energy origin is taken as $\Omega+\epsilon_c$, consistent with Fig. 2. In (b) to (d), the horizontal axis represents the energy loss denoted by $\Omega_1-\Omega_2$, and the excitation energies are marked by the arrows in (a).

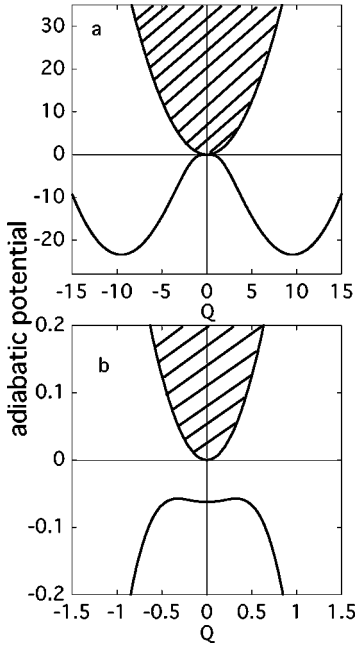

FIG. 4. Adiabatic potential curves along Q for $B=30$: (a) overall feature and (b) expanded feature. The origin of the energy is taken $-\epsilon_c-B$, the bottom of the conduction band. The energy and the length units are the same as in Fig. 2.

luminescence that originates from the Franck-Condon transition from the phonon wave packet that slides down the adiabatic potential curve.[20] The intensity decreases rapidly toward the lower energy side because the wave packet accelerates and because the population in the excited states decreases due to the Auger decay. The hump in the lowest energy part corresponds to the hot luminescence from the classical turning point of the lattice oscillation. The overall features of the line shape are essentially the same for excitations below [Fig. 3(b)] and above [Fig. 3(d)] the absorption peak, although the Rayleigh line becomes slightly prominent.

Now we consider the situation when the excited electron can quantum mechanically itinerate over the entire crystal with a large B. In the one-dimensional system treated here, at least a one bound state, i.e., core exciton state, appears below the conduction band at $Q=0$. The number of the bound states at $Q=0$ critically depends on the ratio of the strength of the core hole potential v to electronic transfer B; there appear a single bound state for $v<B$ and two bound states for $v>B$. A symmetric bound state $|s\rangle$ always emerges below the conduction band, but the asymmetric bound state can appear only for $v/B>1$.

We show the adiabatic potential curves along Q for the parameters $B=30\omega, v=1.0\omega, \alpha=7$ in Fig. 4 where a shaded area represents the conduction band continuum. At $Q=0$, there appears a single bound state below the conduction band with a small binding energy evaluated by $E_B|_{Q=0}=2\omega B\tilde{v}^2/(1+2\tilde{v})\simeq 0.06\omega$, where $\tilde{v}\equiv v/B$. The present parameters give the same lattice relaxation energy as in the localized model. We have two equivalent potential minima both on the positive and negative side of Q, corresponding to the localization of the excited electron on the state $|1\rangle$ and $|2\rangle$, respectively. The feature around $Q=0$, however, is quite different from those seen in the localized model. When we take a closer look around $Q=0$, we can find that the bound core exciton state is locally stable against Q [Fig. 4(b)]. Indeed we can prove that for $v/B<1$ the single core exciton state becomes locally stable as long as the condition

$$S/B\equiv\omega\alpha^2/B\leqslant\{(1+2\tilde{v}^2)/[16\tilde{v}(1+\tilde{v})]\} \qquad (13)$$

is satisfied.

We show in Fig. 5(a) the calculated absorption spectrum due to the transition around the bottom of the conduction band. In Fig. 5(a), the origin of the x-ray energies are taken $-\epsilon_c-B$, i.e., $\Omega=0$ corresponds to the transition to the bottom of the conduction band. The sharp absorption peak is attributed to the transition to the bound core exciton state, which is followed by the continuous absorption band corresponding to the transition to the conduction band.

Since the transition to the s-like single bound state is dipole forbidden as mentioned in Sec. 1, the transition to this state becomes allowed due to the quasi-Jahn-Teller coupling with the conduction band state through the antisymmetric vibration Q. It should be noted that the absorption peak is rather sharp in spite of the large electron phonon interaction which gives the same phonon relaxation energy $S\sim 25\omega$ as

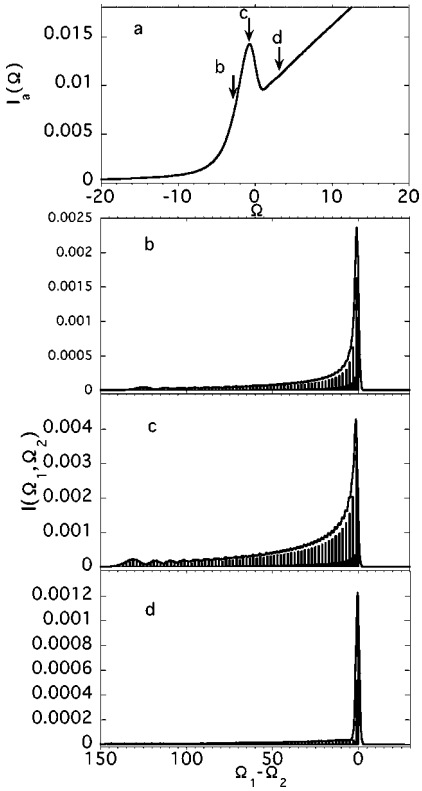

FIG. 5. Calculated results of x-ray absorption (a) and resonant x-ray emission spectra (b)$\sim$(d) for the $B=30$ case. In (a) the horizontal axis is x-ray energy for which the energy origin is taken as $\Omega+\epsilon_c$, consistent with Fig. 4. In (b) to (d), the horizontal axis represents the energy loss denoted by $\Omega_1-\Omega_2$, and the excitation energies are marked by the arrows in (a).

in Fig. 3(a). This indicates that the large itinerancy of the excited electron suppresses the electron-phonon interaction so much that the system behaves as a weak coupling system right after the core excitation.

The resonant x-ray emission spectra for the various excitation energies are shown in Figs. 5(b)–5(d), where the excitation energies are indicated by the arrows. Just at the resonant excitation to the core exciton state (c), the long, low energy tail appears as seen in the localized model where the electron is strongly coupled with the antisymmetric local phonon mode Q. The spectral shape for the lower energy excitation (b) is essentially the same, though the elastic Rayleigh line is slightly more prominent. The fact that the absorption spectrum shows a feature of the weak coupling system on one hand, and the emission spectral feature is characteristic of a strong coupling system on the other, clearly reveals that the changeover from the weak to the strong cooling takes place in a very short time scale of the order of 10 fsec.

Moreover, the low energy tail in Fig. 5(b) is more prominent than that in the localized model [Fig. 3(b)], even though the lattice relaxation energies S and the population decay rate γ of the core excited state are the same for both cases. This is also a consequence of the changeover from the weak to strong coupling regime: The radiative transition decay rate increases with the relaxation because the wave function of the excited electron becomes more localized as the relaxation proceeds.

It should be noted that the situation is quite different in the case of the higher energy excitation in Fig. 5, which should be compared to the higher energy excitation of the localized model [Fig. 3(d)]. Here, the x-ray emission spectrum has only the light scattering components of the Rayleigh and of the lower order Raman lines. This is because the excited electron is diffused away instantaneously all over the crystal, so that the lattice system cannot fully respond to the excitation. The characteristic time scale of the electron migration is of the order of $1/B$, which is much faster than the timescale of the lattice deformation $1/\omega$. The experimental results obtained by Harada *et al.*[2] are consistent with the present calculation.

IV. SUMMARY

We have proposed a model of core excitons with a strong quasi-Jahn-Teller electron phonon coupling system. The theoretical treatment to calculate the resonant x-ray emission as well as x-ray absorption spectrum have been presented. The effect of the quantum electron diffusion is fully incorporated into the model in terms of the lattice Green's function, which makes it possible to quantum mechanically treat the phonon degrees of freedom. This is essentially important when the nonadiabatic transition between the core excited states occurs.

The changeover from the weak to the strong coupling regime during the relaxation is well reflected in the spectral feature: A long energy tail appears in the x-ray emission spectrum at the resonant excitation to the core exciton state, while we have a sharp absorption line for the state. The electronic itinerant effect becomes significant when we go to the higher energy excitation.

In the x-ray absorption experiments with graphite, no distinct peak has been observed below the main peak due to the core exciton state.[2] In the localized model, however, we would have a structure of phonon-assisted transition line below the main peak corresponding to the symmetric core exciton state. The present calculation suggests that the quantum diffusion of the excited electron is decisive to determine the absorption spectral feature.

Here we have shown only the result for $T=0$. However, there is no difficulty to take into acccount the effect of a finite temperature through the Boltzmann distribution of the initial state. Even in this case, the spectral features would not be expected to be more changed than they would be in the localized model because the energy fluctuation in the core excited state is largely reduced by the electronic itinerancy as seen in Fig. 4.

The extension of the present method to a more realistic, higher dimensional system like graphite or diamond is straightforward. In this case we expect a strong polarization dependence in the spectra which is a direct signature of the symmetry breaking of the core excited states due to the vibronic coupling with asymmetric vibrations.[2] The result will be shown in the forthcoming paper.

ACKNOWLEDGMENTS

We wish to thank Y. Harada and S. Shin for valuable discussions. This work is stimulated by the recent experimental results of Ref. 2 performed by them. This work was supported by the Grant-in-Aid for Scientific Research from the Ministry of Education, Science, Sports, and Culture of Japan.

APPENDIX A: ONE-BAND MODEL OF SEMICONDUCTORS

We start from the tight binding model of a one-dimensional semiconductor composed of atoms with an s state and a p_x state, where the x axis is in the direction of the chain with lattice constant d. The Hamiltonian is given by

$$H = -v\sum_j (a_{j,R}^\dagger a_{j,L} + a_{j,L}^\dagger a_{j,R}) - V\sum_j (a_{j,R}^\dagger a_{j+1,L} + a_{j,L+1}^\dagger a_{j,R}), \tag{A1}$$

where $a_{j,R}$ and $a_{j,L}$ are the annihilation operators for the sp hybridized state at jth atom given by

$$a_{j,R} = (1/\sqrt{2})(a_{j,s} + a_{j,p}), \tag{A2}$$

$$a_{j,L} = (1/\sqrt{2})(a_{j,s} - a_{j,p}), \tag{A3}$$

in terms of the annihilation operators for the s state $a_{j,s}$ and the p_x state $a_{j,p}$, respectively. The intra-atomic transfer integral v is related with the energy difference ϵ_{ps} between the p_x state and s state through $v=\epsilon_{ps}/2$. The second term of Eq. (A1) represents the covalent bonding with the interatomic transfer integral $V(>v)$. The magnitude of V may be evaluated through the formula $V=(V_{pp,\sigma}+2V_{sp,\sigma}-V_{ss,\sigma})/2$ and the table of Harrison,[21] for example.

The eigenvalue problem for the above Hamiltonian can be easily solved by the usual procedure. The energy band splits into two, the conduction band and the valence band, the eigenenergies of which are given by

$$E_k^{(\pm)} = \pm\sqrt{v^2 + V^2 + 2vV\cos kd} \tag{A4}$$

for the wave number k, $0 \leqslant k \leqslant 2\pi$. If we write the eigenstates as

$$|\Psi_k^{(\pm)}\rangle = \sum_j \exp(ikdj)(C_k^{(\pm)} a_{j,L}^\dagger|0\rangle + D_k^{(\pm)} a_{j,R}^\dagger|0\rangle), \tag{A5}$$

with $|0\rangle$ being the vacuum of the electron, the coefficients are given by

$$C_k^{(\pm)} = \mp\left(\frac{1}{\sqrt{2}}\right)\frac{v + V\exp(-ikd)}{E_k^{(+)}} \tag{A6}$$

$$D_k^{(\pm)} = \frac{1}{\sqrt{2}}. \tag{A7}$$

In the case $V \gg v$, we can approximately set $C_k^{(\pm)} \simeq \mp(1/\sqrt{2})e^{-ikd}$ and $E_k^{(\pm)} \simeq \pm(V+v\cos kd)$. Therefore, the conduction band has a width $2v$, and the band gap with magnitude $2(V-v)$ is located at $k=\pi/d$. The wave function of the conduction band is given by

$$|\Psi_k^{(+)}\rangle = \sum_j e^{ikdj} a_j^\dagger|0\rangle, \tag{A8}$$

where

$$a_j^\dagger \equiv (a_{j,R}^\dagger - a_{j+1,L}^\dagger)/\sqrt{2} \tag{A9}$$

is the creation operator for the antibonding orbital between the atom j and $j+1$. If we change the phase as $a_j \to (-1)^j a_j$ in order to shift the origin of the wave number k and set $t \equiv v/2$ we obtain the effective Hamiltonian given in Eq. (2b). It can easily be shown that the bottom of the conduction band is made of a linear combination of pure s state.

APPENDIX B: EXPLICIT EXPRESSION OF THE HIERARCHY OF THE EQUATION OF MOTION OF GREEN FUNCTION

We shall derive here a recurrence formula for the phonon Green's function for the relevant electronic components which are necessary to calculate the XAS and RXES spectra.

What we need in the calculation of the spectra are the following components of the resolvent [see Eqs. (6) and (10b)],

$$F_{0;n}(z) \equiv G_n^{1,1}(z) = \langle 1;n|[1/(z-\hat{H}_e)]|1;0\rangle, \tag{B1a}$$

$$F_{1;n}(z) \equiv G_n^{2,1}(z) = \langle 2;n|[1/(z-\hat{H}_e)]|1;0\rangle. \tag{B1b}$$

For the resolvent in Eq. (B1) we apply the Dyson equation

$$\frac{1}{z-\hat{H}_e} = \frac{1}{z-\hat{H}_0} + \frac{1}{z-\hat{H}_0}\hat{V}\frac{1}{z-\hat{H}_e}, \tag{B2}$$

and use the explicit form for the local perturbation V defined in Eq. (2d). We then have the following the recurrence formula: For $n=0$,

$$\begin{aligned} F_{0;n=0}(z) = {} & g_0(z) - v(g_0(z)F_{0;0}(z) + g_1(z)F_{0;1}(z)) \\ & - \alpha\omega(g_0(z)F_{0;0}(z) - g_1(z)F_{0;1}(z)), \end{aligned} \tag{B3a}$$

$$\begin{aligned} F_{1;n=0}(z) = {} & g_1(z) - v(g_1(z)F_{0;0}(z) + g_0(z)F_{0;1}(z)) \\ & - \alpha\omega(g_1(z)F_{0;0}(z) - g_0(z)F_{0;1}(z)), \end{aligned} \tag{B3b}$$

and for $n=1,2,\cdots\infty$,

$$\begin{aligned} F_{0;n}(z) = {} & -v(g_0(z-n\omega)F_{0;n}(z) + g_1(z-n\omega)F_{1;n}(z)) \\ & - \alpha\omega(g_0(z-n\omega)[\sqrt{n+1}F_{0;n+1}(z) + \sqrt{n}F_{0;n-1}(z)] \\ & - g_1(z)[\sqrt{n+1}F_{1;n+1}(z) + \sqrt{n}F_{0;n-1}(z)]), \end{aligned} \tag{B4a}$$

$$\begin{aligned} F_{1;n}(z) = {} & -v(g_1(z-n\omega)F_{0;n}(z) + g_0(z-n\omega)F_{1;n}(z)) \\ & - \alpha\omega(g_0(z-n\omega)[\sqrt{n+1}F_{0;n+1}(z) + \sqrt{n}F_{0;n-1}(z)] \\ & - g_0(z)[\sqrt{n+1}F_{1;n+1}(z) + \sqrt{n}F_{1;n-1}(z)]), \end{aligned} \tag{B4b}$$

where $g_0(z)$ and $g_1(z)$ are the components of the lattice Green's functions.

Eqs. (B3) and (B4) may be expressed in a compact way,

$$\mathbf{F}_n(z) = \delta_{n,0}\begin{bmatrix} g_0(z) \\ g_1(z) \end{bmatrix} - v\begin{bmatrix} g_0(z-n\omega) & g_1(z-n\omega) \\ g_1(z-n\omega) & g_0(z-n\omega) \end{bmatrix} \mathbf{F}_n(z) - \alpha\omega\begin{bmatrix} g_0(z-n\omega) & g_1(z-n\omega) \\ g_1(z-n\omega) & g_0(z-n\omega) \end{bmatrix} \{\sqrt{n}\mathbf{F}_{n-1}(z) + \sqrt{n+1}\mathbf{F}_{n+1}(z)\}, \quad \text{(B5)}$$

where the components of the vector $\mathrm{F}_n(z)$ are given in Eq. (B3),

$$\mathbf{F}_n(z) \equiv \begin{bmatrix} F_{0,n}(z) \\ F_{1,n}(z) \end{bmatrix}. \quad \text{(B6)}$$

Note that the first term in the curly bracket in Eq. (B4b) should be dropped for $n=0$.

The infinite series of Eq. (B5) can be truncated at a large value of n, for which the spectral function is converged well. The closed equation for $\mathbf{F}$ is numerically solved by the conjugate gradient method.

*Electronic address: stanaka@ms.cias.osakafu-u.ac.jp

[1] Y. Ma, P. Skytt, N. Wassdahl, P. Glans, D. C. Mancini, J. Guo, and J. Nordgren, Phys. Rev. Lett. **71**, 3725 (1993).

[2] Y. Harada, T. Tokushima, Y. Takata, T. Takeuchi, Y. Kitajima, S. Tanaka, Y. Kayanuma, and S. Shin, Phys. Rev. Lett. **93**, 017 401 (2004).

[3] A. B. Preobrajenski, A. S. Vinogradov, S. L. Molodtsov, S. K. Krasnikov, T. Chasse, R. Szargan, and C. Laubschat, Phys. Rev. B **65**, 205116 (2002).

[4] F. Gel'mukhanov and H. Ågren, Phys. Rep. **312**, 87 (1999).

[5] K. Ueda, J. Electron Spectrosc. Relat. Phenom. **88–91**, 1 (1998).

[6] M. Simon, C. Miron, N. Leclercq, P. Morin, K. Ueda, Y. Sato, S. Tanaka, and Y. Kayanuma, Phys. Rev. Lett. **79**, 3857 (1997).

[7] K. Ueda, M. Simon, C. Miron, N. Leclercq, R. Guillemin, P. Morin, and S. Tanaka, Phys. Rev. Lett. **83**, 3800 (1999).

[8] K. Ueda, S. Tanaka, Y. Shimizu, Y. Muramatsu, H. Chiba, T. Hayaishi, M. Kitajima, and H. Tanaka, Phys. Rev. Lett. **85**, 3129 (2000).

[9] H. Yoshida, K. Nobusada, K. Okada, S. Tanimoto, N. Saito, A. De Fanis, and K. Ueda, Phys. Rev. Lett. **88**, 083 001 (2002).

[10] S. Tanaka and Y. Kayanuma, Solid State Commun. **64**, 77 (1996).

[11] J. F. Morar, F. J. Himpsel, G. Hollinger, G. Hughes, and J. L. Jordan, Phys. Rev. Lett. **54**, 1960 (1985).

[12] K. A. Jackson and M. R. Pederson, Phys. Rev. Lett. **67**, 2521 (1991).

[13] D. A. Fischer, R. M. Wentzcovitch, R. G. Carr, A. Continenza, and A. J. Freeman, Phys. Rev. B **44**, 1427 (1991).

[14] P. E. Batson, Phys. Rev. B **48**, 2608 (1993).

[15] P. A. Brühwiler, A. J. Maxwell, C. Puglia, A. Nilsson, S. Andersson, and N. Nordgren, Phys. Rev. Lett. **74**, 614 (1995).

[16] J. Nordgren, P. Glans, K. Gunnelin, J. Guo, P. Skytt, C. Sather, and N. Wassdahl, Appl. Phys. (N.Y.) **65**, 97 (1997).

[17] Y. Kayanuma and S. Tanaka, J. Electron Spectrosc. Relat. Phenom. **136**, 167 (2004).

[18] W. H. Press, W. T. Vetterling, S. A. Teukolsky, and B. P. Flannery, *Numerical Recipes in Fortran 77: The Art of Scientific Computing* (Cambridge University Press, 1992).

[19] Y. Toyozawa, *Optical Processes in Solids* (Cambridge University Press, 2003).

[20] Y. Kayanuma, J. Phys. Soc. Jpn. **57**, 292 (1988).

[21] W. A. Harrison, *Electronic Structures and the Properties of Solids: The Physcs of Chemical Bond* (Dover, New York, 1989), Solid State Table of Elements.